Mathematisch-Naturwissenschaftliche Fakultät
Ernst Moritz Arndt Universität Greifswald

Bachelor Thesis

Non-linear Monte Carlo methods for neutrals

Jonathan Klingelhöfer

July 11, 2014

First Supervisor:
Prof. Dr. Ralf Schneider

Second Supervisor:
PD Dr. Berndt Bruhn

Eidesstattliche Erklärung

Ich versichere, dass ich die vorliegende Bachelorarbeit selbständig verfasst und keine anderen Hilfsmittel als die angegebenen verwendet habe. Die Stellen, die anderen Werken dem Wortlaut oder dem Sinne nach entnommen sind, habe ich in jedem Falle durch Angaben der Quelle, auch der Sekundärliteratur, als Entlehnung kenntlich gemacht.

Greifswald, den 11.07.2014

Contents

1. Introduction

The Direct Simulation Monte Carlo (DSMC) method is used to simulate neutral particle dynamics in fluids of low density, where continuous models fail [1, pp. 203ff] [2] [3]. It is a kinetic method to approximate the collective behaviour of particle dynamics. For this, a large number of particles of one species is combined into one pseudo-particle. This number is called *weight* of the pseudo-particle. The trajectories of pseudo-particles are determined by their equation of motion. For particles in electric or magnetic fields these trajectories of pseudo-particles are identical to the trajectories of the individual particles, because only the charge-to-mass ratio contributes to the acceleration due to the Lorentz force. Neutral particles with zero charge are included here, too. The interactions between particles on small length scales are simulated through a model of binary collisions using random numbers. The model is valid for fluids of low density.

There are many physical systems that can be simulated with DSMC containing more than one particle species. Many of these systems might contain a trace species which significantly affects the behaviour of the whole system e.g. a slightly ionized plasma or a reactive gas mixture. For simulating such systems it is essential to carry a statistically meaningful number of pseudo-particles of the trace species. For conventional DSMC methods the weight of all pseudo-particles is identical, as the binary collision model only yields correct results for equal pseudo-particle weights. For a correct statistical representation in a system with trace species, identical weights means low weights for all pseudo-particles. But low weights for all pseudo-particles lead to a large number of non-trace pseudo-particles that results in significant computational effort without contributing appreciable information. In other words, the trace species' weight needs to be lower than that of the majority species for an acceptable computational effort.

Hence, conventional DSMC needs to be improved to variable pseudo-particle weights as initiated by G. A. Bird [1, pp. 215f] and carried on by I. D. Boyd [2]. The purpose of this bachelor thesis is to evaluate different methods that extend DSMC to variable pseudo-particle weights. The consequences for distribution functions and energy or linear momentum conservation are discussed for the different approaches.

After introducing the physical principles for DSMC, the algorithmic details of DSMC are discussed and existing concepts for non-linear weighting schemes are introduced. These concepts are extended in chapter four by own ideas. In chapter five the numerical results of some physical test cases using the previously discussed methods for non-linear DSMC are evaluated. It follows a short conclusion and a prospect of further developments in chapter six.

2. Physical principles

To understand DSMC it is necessary to become familiar with some basics about distribution functions and with the binary collision model. A standard method to model interactions between neutrals, the hard sphere model, will be explained.

2.1. Distribution functions

In classical physics a many-particle system can be described by its distribution function $\varrho(q_k, p_k, t)$, where q_k and p_k are the generalized coordinates and momenta with $k \in \{1, \ldots, 3N\}$ where $3N$ is the number of degrees of freedom [4]. The expectation value of a physical quantity A, like a particle's velocity or energy, is given by the integral

$$\langle A \rangle = \int \varrho \cdot A \cdot \mathrm{d}^{3N}q \ \mathrm{d}^{3N}p \ . \tag{2.1}$$

For a finite number N of particles with position $\vec{r}_k$ and linear momentum $\vec{p}_k$ the integral form of the expectation value becomes a discrete sum over a discrete distribution function ϱ_d, so

$$\langle A \rangle = \sum_{k=1}^{N} A \cdot \varrho_d \left(\vec{r}_k, \vec{p}_k\right) \ . \tag{2.2}$$

2.1.1. Maxwell-Boltzmann distribution

According to Boltzmann's H-theorem for ideal fluids in thermodynamic equilibrium the distribution function turns through collision processes into a normal distribution in velocity, which is called *Maxwell-Boltzmann distribution*:

$$\varrho(v_x, v_y, v_z) = \left(\frac{m}{2\pi k_B T}\right)^{3/2} \cdot \exp\left(-\frac{m(v_x^2 + v_y^2 + v_z^2)}{2k_B T}\right) \tag{2.3}$$

with the Boltzmann constant k_B and the absolute temperature T. A detailed derivation can be found in [1, pp. 61ff]. Using polar coordinates in velocity space it also can be written as a distribution function of the absolute value $v = \sqrt{v_x^2 + v_y^2 + v_z^2}$ of velocity. Taking the Jacobian determinant into account integrating over the azimuthal and meridian angles the Maxwell-Boltzmann distribution becomes

$$\varrho(v) = 4\pi \cdot \left(\frac{m}{2\pi k_B T}\right)^{3/2} \cdot v^2 \cdot \exp\left(-\frac{mv^2}{2k_B T}\right) \ . \tag{2.4}$$

2.1.2. Important velocities in a Maxwell-Boltzmann distributed gas

According to the principle of (2.1) the first and second moment of v can be calculated. The expectation value of v is

$$\langle v \rangle = \int_0^\infty v \cdot \varrho(v) \, \mathrm{d}v = \sqrt{\frac{8k_B T}{\pi m}}. \tag{2.5}$$

The second moment is calculated as the expectation value of v^2

$$\langle v^2 \rangle = \int_0^\infty v^2 \cdot \varrho(v)\,\mathrm{d}v = \frac{3k_B T}{m} \quad . \tag{2.6}$$

Analogously, the expectation value of the relative velocity between two particles subscripted with 1 and 2 can be calculated as

$$\langle v_r \rangle = \left\langle \sqrt{\left(v_{x,1} - v_{x,2}\right)^2 + \left(v_{y,1} - v_{y,2}\right)^2 + \left(v_{z,1} - v_{z,2}\right)^2} \right\rangle \tag{2.7}$$

$$= \int v_r(v_{i,1}, v_{i,2}) \cdot \varrho(v_{i,1}) \cdot \varrho(v_{i,2})\,\mathrm{d}^3 v_{i,1} \mathrm{d}^3 v_{i,2} = \sqrt{2} \cdot \langle v \rangle \quad . \tag{2.8}$$

2.2. Model of binary collision

For a statistically correct simulation of interaction processes between gas particles using random numbers, it is necessary to know the reaction probability for the particular interaction process and the mean collision number, respectively. If the density of the gas is low enough, it can be assumed that a particle never interacts with more than one other particle so that only binary collisions take place [3] [4]. Hence, this approach is called *model of binary collision*. The big advantage of the model is that a binary collision process can be described completely with analytic methods.

2.2.1. Elastic binary collision

Elastic scattering is characterized by conservation of energy and of course by conservation of linear momentum. Two-particle interactions are described in the center-of-mass frame such that the velocities $\vec{v}_1$ and $\vec{v}_2$ of particles with masses m_1 and m_2 transform to relative velocity $\vec{v}_r$ and center-of-mass velocity $\vec{V}$ as [5, pp. 17-22]

$$\vec{v}_r = \vec{v}_1 - \vec{v}_2 \qquad \text{and} \qquad \vec{V} = \frac{m_1 \vec{v}_1 + m_2 \vec{v}_2}{m_1 + m_2} \quad . \tag{2.9}$$

Conservation of linear momentum thus becomes equivalent to $\dot{\vec{V}} = 0$. Conservation of energy on the other hand can be written as

$$\dot{E} = \frac{m_1 \cdot m_2}{m_1 + m_2} \cdot \vec{v}_r \cdot \dot{\vec{v}}_r = 0 \quad . \tag{2.10}$$

So any elastic binary collision is described by a rotation of the relative velocity $\vec{v}_r$. Therefore, the velocities after the collision can be written as

$$\vec{v}_1' = \vec{V}' + \frac{m_2}{M}\vec{v}_r' = \vec{V} + \frac{m_2}{M}\hat{A} \cdot \vec{v}_r = \vec{v}_1 + \frac{m_2}{M} \cdot \left(\hat{A} - \hat{1}\right)\vec{v}_r = \vec{v}_1 + \frac{m_2}{M} \cdot \Delta\vec{v}_r \tag{2.11}$$

$$\vec{v}_2' = \vec{V}' - \frac{m_1}{M}\vec{v}_r' = \vec{V} - \frac{m_1}{M}\hat{A} \cdot \vec{v}_r = \vec{v}_2 - \frac{m_1}{M} \cdot \left(\hat{A} - \hat{1}\right)\vec{v}_r = \vec{v}_2 - \frac{m_1}{M} \cdot \Delta\vec{v}_r \quad , \tag{2.12}$$

where the prime $'$ indicates post-collision properties, $M = m_1 + m_2$, $\hat{A}$ is a rotation matrix with $\det \hat{A} = 1$ and $\hat{1}$ is the identity matrix. The generalization to inelastic collisions is performed by maintaining momentum conservation and demanding $\dot{E} < 0$ such that $\vec{v}_r$ is rotated and decreased in absolute value.
For writing $\hat{A}$ as a function of azimuthal angle φ and scattering angle θ consider the transformation of $\vec{v}_r$ into relative velocity coordinate frame (see Figure 2.1) by

$$\widetilde{\vec{v}_r} = v_r \cdot \vec{e}_z = \hat{R}(\psi, \xi) \cdot \vec{v}_r \quad , \tag{2.13}$$

where $\hat{R}(\psi, \xi)$ is given by

$$\hat{R}(\psi, \xi) = \begin{bmatrix} \cos\xi\cos\psi & \cos\xi\sin\psi & -\sin\xi \\ -\sin\psi & \cos\psi & 0 \\ \sin\xi\cos\psi & \sin\xi\sin\psi & \cos\xi \end{bmatrix} \tag{2.14}$$

with

$$\cos\xi = \frac{(\vec{v}_r)_z}{v_r} \quad \text{and} \quad \tan\psi = \frac{(\vec{v}_r)_y}{(\vec{v}_r)_x} \ . \tag{2.15}$$

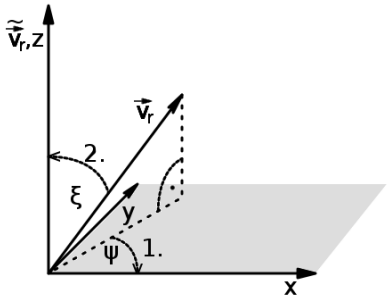

Figure 2.1.: Transformation of $\vec{v}_r$ into the relative velocity coordinate frame.

In this frame (denoted by the wave $\tilde{}$) rotation of relative velocity by azimuthal angle φ and scattering angle θ arises (see Figure 2.2) as

$$\tilde{\vec{v}}_r{}' = \hat{R}^T(\varphi, \theta)\tilde{\vec{v}}_r = \tilde{\hat{A}}\,\tilde{\vec{v}}_r \ , \tag{2.16}$$

where $\hat{R}^T$ is the transpose of $\hat{R}$ and the inverse respectively, such that $\hat{A}$ simply becomes

$$\hat{A} = \hat{R}^T(\psi, \xi) \cdot \hat{R}^T(\varphi, \theta) \cdot \hat{R}(\psi, \xi) \ . \tag{2.17}$$

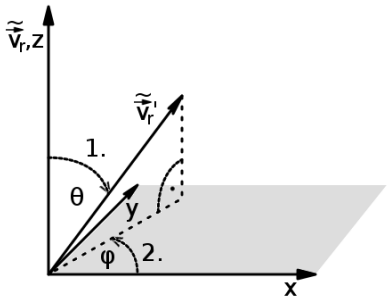

Figure 2.2.: Rotation of $\tilde{\vec{v}}_r$ by scattering angle θ and azimuthal angle φ in relative velocity coordinate frame. The rotation is the same as in Figure 2.1 but with opposite directions.

2.2.2. Reaction probability, cross section

To derive the reaction probability one considers a gas with particle number N occupying a fixed volume V such that the particle number density is $n = N \cdot V^{-1}$ [1, pp. 7f]. In the model of binary collsion, it is reasonable to assume that a reaction between two particles with relative velocity v_r takes place if, and only if, during the time interval Δt both particles are located in the same volume element $\sigma \cdot v_r \cdot \Delta t$ with base area σ (see figure 2.3). This depends on the relative velocity v_r. The reaction probability P_R between the two particles then can be written as the ratio of the volumes

$$P_R(v_r) = \frac{\sigma(v_r) \cdot v_r \cdot \Delta t}{V} \quad . \tag{2.18}$$

The base area σ of the volume element is defined as *cross section*.

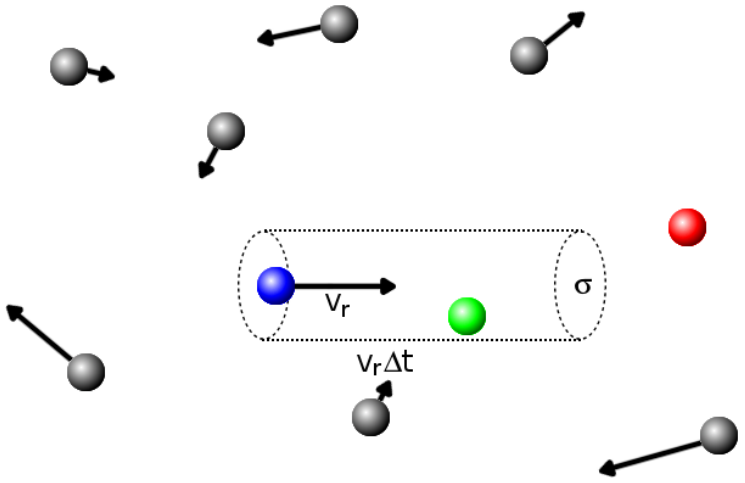

Figure 2.3.: Rest frame of both the green and the red particle, which have the same relative velocity v_r to the blue particle. But only the green particle is located in the volume $\sigma \cdot v_r \cdot \Delta t$ around the blue particle and thus the green and the blue will collide during Δt while the red and the blue will not.

2.2.3. Differential cross section

In many cases the differential cross section is of further interest delivering probabilities for scattering into a spatial direction. It is defined as [1, p. 34]

$$\frac{\mathrm{d}\sigma}{\mathrm{d}\Omega}\mathrm{d}\Omega = b\,\mathrm{d}b\,\mathrm{d}\varphi \quad . \tag{2.19}$$

Here, b is the distance of closest approach, also called *impact parameter*, $\mathrm{d}\Omega$ the solid angle element in which a particle is scattered and $\mathrm{d}\varphi$ the azimuthal angle element of the location of the incident particle. After substituting $\mathrm{d}\Omega = \sin(\theta)\,\mathrm{d}\theta\,\mathrm{d}\varphi$, (2.19) becomes

$$\frac{\mathrm{d}\sigma}{\mathrm{d}\Omega} = \frac{b}{\sin(\theta)} \left| \frac{\mathrm{d}b}{\mathrm{d}\theta} \right| \quad . \tag{2.20}$$

2.2.4. Mean collision numbers

Any gas particle could react with any other particle in the volume. The total collision probability, which is also the expectation value of the total number of collisions $\langle N_c \rangle$, is the sum of all

individual collision probabilities [1, pp. 7f, 219f]. Hence the mean number of collisions $\langle N_c \rangle^s$ for one single particle using $N - 1 \simeq N$ is

$$\langle N_c \rangle^s = \sum_{k=2}^{N} P_R(v_r(1,k)) = \left(\sum_{k=2}^{N} 1 \right) \frac{\Delta t}{V} \cdot \langle \sigma v_r \rangle^s = \frac{N-1}{V} \Delta t \cdot \langle \sigma v_r \rangle^s \simeq n \Delta t \cdot \langle \sigma v_r \rangle^s \tag{2.21}$$

and altogether the mean number of collisions is

$$\langle N_c \rangle = \sum_{i=1}^{N-1} \sum_{k=i+1}^{N} P_R^{i,k} = \left(\sum_{i=1}^{N-1} \sum_{k=i+1}^{N} 1 \right) \langle P_R \rangle = \frac{N(N-1)}{2V} \Delta t \cdot \langle \sigma v_r \rangle \simeq \frac{Nn}{2} \Delta t \cdot \langle \sigma v_r \rangle \ . \tag{2.22}$$

Here, $\langle \sigma v_r \rangle$ is the average of all products $\sigma^{(i,k)} v_r^{(i,k)}$ of particles i and k. If there are not just one but two types of gas components, the upper limits in (2.22) have to be replaced by the total number of particles in the volume of both types N_1, N_2 and the second summation has to start with $k = 1$. Besides the supplement $^{1 \leftrightarrow 2}$ will be introduced to indicate the number of collisions between species 1 and 2. Analogously to the calculation above

$$\langle N_c \rangle^{s\,1 \leftrightarrow 2} = n_2 \Delta t \cdot \langle \sigma v_r \rangle^{s\,1 \leftrightarrow 2} \ . \tag{2.23}$$

is the number of collisions for one single particle of species 1 with the particles of species 2 and

$$\langle N_c \rangle^{1 \leftrightarrow 2} = N_1 n_2 \Delta t \cdot \langle \sigma v_r \rangle^{1 \leftrightarrow 2} \ . \tag{2.24}$$

is the number of collisions between all particles of species 1 with species 2, respectively.

2.2.5. Mean collision time, mean free path

Knowing the mean collision number in the time interval Δt for one single particle of species 1, a *collision frequency* can be defined by division of $\langle N_c \rangle^s + \langle N_c \rangle^{s\,1 \leftrightarrow 2} + ... + \langle N_c \rangle^{s\,1 \leftrightarrow M}$ given by (2.21) and (2.23) through Δt [1, pp. 7f]. Taking the reciprocal value instead defines the *mean collision time* τ a particle of species 1 moves without collision:

$$\tau = \frac{\Delta t}{\sum \langle N_c \rangle^s} \simeq \frac{1}{n \cdot \langle \langle \sigma v_r \rangle^s \rangle} \ . \tag{2.25}$$

Multiplying the mean velocity $\langle v \rangle$ in (2.5) by the mean collision time τ yields the *mean free path* λ_{mfp}. As the name implies, λ_{mfp} is the distance a particle of species 1 covers on average without a collision. For a gas containing only one species it is calculated as

$$\lambda_{\mathrm{mfp}} = \langle v \rangle \cdot \tau = \frac{1}{n} \cdot \frac{\langle v \rangle}{\langle \langle \sigma v_r \rangle^s \rangle} \ . \tag{2.26}$$

2.3. Application to the model of colliding hard spheres

One model for collisions that is often used to describe the interactions of neutrals is the hard sphere model. Here, two particles are considered as hard spheres that collide elastically like billard balls. There is no interaction unless both spheres contact each other at their surfaces. As the Lennard-Jones potential that causes repulsion between neutrals scales like r^{-12} with distance r the hard-sphere model yields good results for many types of neutrals [4].

2.3.1. Derivation of the cross section

The angle of reflection has the same absolute value as the angle of incidence $\theta/2$ (see Figure 2.4). The impact parameter b then depends on the mean d_{12} of the diameters of both spheres and on the scattering angle θ like [1, p. 39]

$$b = d_{12} \cdot \sin\left(\frac{\theta}{2} \right) \ . \tag{2.27}$$

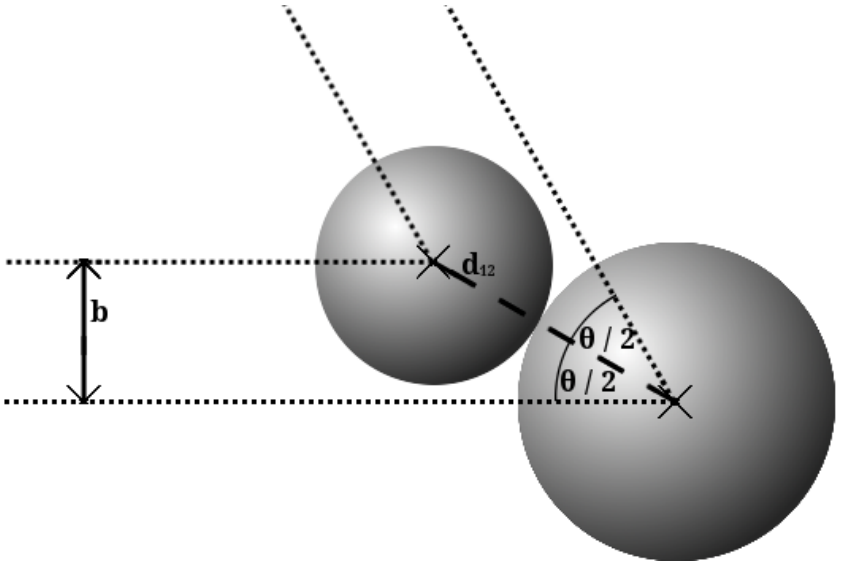

Figure 2.4.: Schematic representation of two colliding hard spheres.

With (2.20) and one trigonometric addition theorem it follows that the differential cross section is constant

$$\frac{\mathrm{d}\sigma}{\mathrm{d}\Omega} = \frac{d_{12}^2}{4} \quad . \tag{2.28}$$

Thus, the total cross section becomes

$$\sigma = \int \frac{\mathrm{d}\sigma}{\mathrm{d}\Omega}\mathrm{d}\Omega = 4\pi \cdot \frac{\mathrm{d}\sigma}{\mathrm{d}\Omega} = \pi \cdot d_{12}^2 \quad . \tag{2.29}$$

2.3.2. Mean free path, mean collision time, limitations of DSMC

Due to the independence of the cross section from relative velocity, the mean free path and the mean collision time can be calculated for a Maxwell-distributed hard-sphere gas exploiting (2.5), (2.7), (2.26), (2.25) and (2.29):

$$\lambda_{\mathrm{mfp}} = \frac{1}{\sqrt{2}n\pi d_{12}^2} \qquad \text{and} \qquad \tau = \frac{1}{4nd_{12}^2}\sqrt{\frac{m}{\pi k_B T}} \quad . \tag{2.30}$$

>From this, the limitations of validity for the binary collision model get clearer. The model is only valid if the mean free path and the mean molecular spacing $n^{-1/3}$ are much greater than the mean molecular diameter $\lambda_{\mathrm{mfp}} \gg d_{12}$, $n^{-1/3} \gg d_{12}$. DSMC can be used safely if $\lambda_{\mathrm{mfp}}/d_{12} \geq 10$ [3, p. 405].

3. Basics of Direct Simulation Monte Carlo

As already mentioned in the beginning, DSMC is a simulation method that uses pseudo-particles that represent a certain number of real particles. This number is called *weight*. In this chapter DSMC is expounded quantitatively for equal pseudo-particle weights W. Later, some existing concepts for differently weighted particles are introduced.
The interactions between the pseudo-particles at DSMC are implemented using the binary collision model and its analytic description introduced in chapter 2.2. For this, the simulation area is divided into cells, where each cell is treated as an independent interaction volume within one time interval Δt of the simulation [1, pp. 218ff] [2] [3, pp. 409ff]. One divides the simulated pseudo-particles of each cell into pairs and let them perform a binary collision according to 2.2.1. Afterwards, each pseudo-particle at location $\vec{r}$ with velocity $\vec{v}$ can be pushed to a new location $\vec{r}' = \vec{r} + \vec{v}\Delta t$.
The number of reactions in (2.21) during the time interval Δt defines the number of pairs which have to be considered for collisions in one simulation time step. The local particle number N has to be replaced by the number of pseudo-particles N/W of each cell and the mean number of collisions $\langle N_c \rangle$ has to be replaced by the cell-specific number of pairs of pseudo-particles $\overline{N}_p \geq \langle N_c \rangle / W$. The overline $\overline{\ }$ indicates, that this number is a number of pseudo-particles, not of real ones. The particle number density n can be claculated by dividing the local number of real particles N through the volume V of the cell.
It is important to note that one simulation time step needs to be of order of the mean collision time and that one cell width needs to be of order of the mean free path. Otherwise, it is not guaranteed that the simulated physics is correct.
As already mentioned above, the cross section is in general a function of relative velocity or, alternatively, of energy. Therefore, it is necessary to replace the average $\langle \sigma v_r \rangle$ in (2.21) by the maximum value. The number of pairs that are considered for a collision is then obtained as

$$\overline{N}_p = \frac{Nn}{2W} \cdot \Delta t \cdot (\sigma v_r)_{\max} \ . \tag{3.1}$$

Not every selected pair is allowed to perform a collision. The reaction probability P_r for each selected pair is given by

$$P_r = \frac{\sigma(v_r) \cdot v_r}{(\sigma v_r)_{\max}} \tag{3.2}$$

with relative velocity v_r. This is then used to decide if a collision is accepted or not. This probabilistic approach means that the number of simulated collisions is not deterministic equal to the average number of collisions in (2.21), but creates a distribution very similar to the real process. The simulation algorithm compares a random number with the collision probability and accepts the collision if the random number is smaller than the probability. The velocity dependent cross section values can be taken from experimental measurements [7].
Care must be taken by calculating the fraction of the number of collisions that cause a scattering with scattering angle within the interval $[\theta, \theta + \mathrm{d}\theta]$. Differentiating (3.1) with respect to θ and dividing the quotient through the initial equation (indicated by index 0) provides

$$\frac{1}{\overline{N}_{p,0}} \frac{\mathrm{d}\overline{N}_p}{\mathrm{d}\theta} = \frac{1}{N_0} \frac{\mathrm{d}N}{\mathrm{d}b} \frac{\mathrm{d}b}{\mathrm{d}\theta} \ . \tag{3.3}$$

As one can see the number of reactions within the interval $[\theta, \theta + \mathrm{d}\theta]$ is not necessarily constant although the differential cross section for hard spheres is. It rather depends on the number of incident particles with impact parameter in the interval $[b, b + \mathrm{d}b]$. If the assumption is that the incident particles are uniformly distributed in the plane perpendicular to the incident direction of motion, their distribution function in b becomes for hard spheres

$$\frac{1}{N_0}\frac{\mathrm{d}N}{\mathrm{d}b} = \frac{2b}{d_{12}^2} \quad . \tag{3.4}$$

Using (2.27) and (3.4) integrating (3.3) yields the probabilty of scattering angle θ within the interval $[0, \theta_{\max}]$ as [5, pp. 27f]

$$P_\theta(0 \leq \theta < \theta_{\max}) = \frac{\Delta N_c(\theta_{\max})}{N_{c,0}} = \frac{1}{2} \cdot (1 - \cos(\theta_{\max})) \quad . \tag{3.5}$$

The assumption of uniformly distributed incident particles also creates an uniform distribution in azimuthal angle φ

$$P_\varphi(0 \leq \varphi < \varphi_{\max}) = \frac{\Delta N_c(\varphi_{\max})}{N_{c,0}} = \frac{\varphi_{\max}}{2\pi} \quad . \tag{3.6}$$

The algorithm for calculating the particle interactions during each simulation time step in each cell for conventional DSMC can now be summarized.

1. Calculate the number of pairs to be considered for collision by (3.1).
2. For each pair choose randomly two particles of the cell.
3. Use a random number to check if the selected pair will collide according to (3.2).
4. Randomly choose the impact angles θ and φ according to (3.5) and (3.6).
5. Calculate the rotation matrix $\hat{A}$ by (2.17).
6. Calculate the post-collision velocities according to (2.11) and (2.12).

3.1. Existing concepts for non-linear weighting schemes

How the DSMC algorithm has to be modified when variable pseudo-particle weights are introduced to save valuable computation resources will be discussed in the following. As the number of pairs considered for collisions is proportional to the number of pseudo-particles N/W, where W is the constant pseudo-particle weight, it can be seen that this number is the first quantity that has to be modified, since W is varied. For this, consider the pseudo-particles with least weight $W_{\min}$. If all particles have this weight the number of pairs will maximally become

$$\overline{N}_p = \frac{Nn}{2W_{\min}} \cdot \Delta t \cdot (\sigma v_r)_{\max} \quad . \tag{3.7}$$

Analogously to the introduction of $(\sigma v_r)_{\max}$ there are now too many pseudo-particles selected for collision. This can be corrected by reducing the reaction-probability. But before this can be done an approach for treating the collision process between two differently weighted particles is needed. For a selected pair of pseudo-particles with weights W_1 and W_2 the minimum of W_1 and W_2 represents the number of real collisions. Thus, the collision probability has to be modified to

$$P_r = \frac{\sigma(v_r) \cdot v_r}{(\sigma v_r)_{\max}} \cdot \frac{W_{\min}}{\min\{W_1, W_2\}} \quad . \tag{3.8}$$

The correctness of this assumption can be proven by calculating the mean number of collisions

$$\begin{aligned}\langle N_c \rangle &= \langle \overline{N}_p \cdot \min\{W_1, W_2\} \cdot P_r \rangle \\ &= \frac{Nn}{2} \cdot \Delta t \cdot \langle \sigma v_r \rangle, \end{aligned} \tag{3.9}$$

which agrees with (2.22). If there are only pseudo-particles with either weight W_1 or W_2 the number of pairs can be divided into a number of pairs between pseudo-particles of equal weight W_1, of equal weight W_2 and of mixed weight W_1 and W_2

$$\overline{N}_p^{1\leftrightarrow 1} = \frac{N_1 n_1}{2W_1} \cdot \Delta t \cdot (\sigma v_r)_{\max} \tag{3.10}$$

$$\overline{N}_p^{1\leftrightarrow 2} = \frac{N_1 n_2}{\min\{W_1, W_2\}} \cdot \Delta t \cdot (\sigma v_r)_{\max} \tag{3.11}$$

$$\overline{N}_p^{2\leftrightarrow 2} = \frac{N_2 n_2}{2W_2} \cdot \Delta t \cdot (\sigma v_r)_{\max} \ . \tag{3.12}$$

Their reaction probabilities then change to

$$P_r^{i\leftrightarrow j} = \frac{\sigma(v_r) \cdot v_r}{(\sigma v_r)_{\max}} \tag{3.13}$$

for any $i, j \in \{1, 2\}$. The advantage is that the number of pairs $\overline{N}_p^{2\leftrightarrow 2}$ can be reduced if $W_2 > W_1$ as $1/W_2 < 1/\min\{W_1, W_2\}$. But the treatment of the collision process itself can not be done superficially as the following discussion will show.

3.1.1. Non-conservative weighting scheme by Bird

One possibility to deal with different particle weights was introduced by G. A. Bird [1, pp. 213f] [2]. It uses the ratio of two different pseudo-particle weights as probabilities to change the properties (momentum and energy) of the higher weighted particle. A big disadvantage of this method is that energy and momentum are not conserved explicitly for any collision but only over a large amount of collisions. As the usage of the non-conservative weighting scheme by Bird is not suggested even by Bird himself the focus now is on conservative weighting schemes or variations of them.

3.1.2. Conservative weighting scheme by Boyd

Another method was introduced by I. D. Boyd [2], where linear momentum is conserved exactly at each collision by splitting a higher weighted particle with weight $\widetilde{W}_1$ into two particles. One of those has the weight of the less weighted collision partner $\widetilde{W}_2$. The equally weighted particles may then collide according to the conventional concept (see figure 3.1). As the purpose of heigher weights is a reduction of calculation time, it is necessary to merge the split particles after the collision process again, because otherwise the number of pseudo-particles and with that the computation time would increase with growing runtime. If the weights of the initial particles are not equal ($\widetilde{W}_1 > \widetilde{W}_2$), there is a loss of energy ΔE in the merging process after the collision. It can be calculated by

$$\Delta E = \widetilde{W}_2 \left(1 - \frac{\widetilde{W}_2}{\widetilde{W}_1}\right) \cdot \frac{m_1}{2} \left(\vec{v}_1 - \vec{v}_1'\right)^2, \tag{3.14}$$

where m_1 is the mass of one particle of species 1, $\vec{v}_1$ is the initial velocity of particle 1 and $\vec{v}_1'$ is the post-collision velocity of the split off part of particle 1. The idea is that the lost energy ΔE is added to the relative velocity of two subsequently colliding particles with equal weight, so that both linear momentum and energy are conserved (see section 4.2.3).

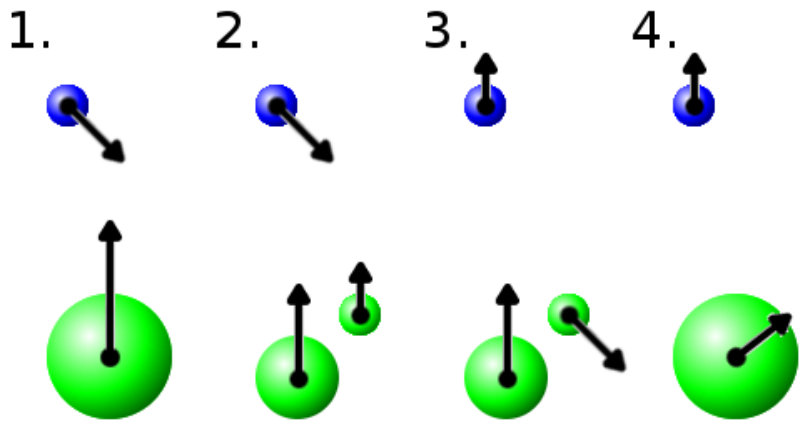

Figure 3.1.: The blue and the green pseudo-particle are selected for collision (1.). Therefore the green pseudo-particle is split into two (2.). Then, the collision for the equally weighted pseudo-particles is performed (3.). Finally, the green pseudo-particles are merged again to one (4.). In all images the radius corresponds with the pseudo-particle's weight.

4. Concepts for non-linear weighting schemes

4.1. Direct conservation of both energy and momentum

As another possibility to deal with differently weighted particles one can collide them directly according to (2.10) to (2.12), where the weights of the particles have to be introduced as a scaling factor of the masses, such that

$$\dot{E} = 0 = \frac{W_1 m_1 \cdot W_2 m_2}{W_1 m_1 + W_2 m_2} \cdot \vec{v}_r \cdot \dot{\vec{v}}_r \ . \tag{4.1}$$

The post-collision velocities then become

$$\vec{v}_1' = \vec{v}_1 + \frac{m_2 W_2}{m_1 W_1 + m_2 W_2} \cdot \Delta\vec{v}_r \tag{4.2}$$

$$\vec{v}_2' = \vec{v}_2 - \frac{m_1 W_1}{m_1 W_1 + m_2 W_2} \cdot \Delta\vec{v}_r \tag{4.3}$$

with

$$\Delta\vec{v}_r = \left(\hat{A} - \hat{1}\right) \vec{v}_r \ . \tag{4.4}$$

At first sight this seems to be a great idea, but the numerical results in chapter 5 will show severe restrictions.

4.2. Variations of the conservative weighting scheme

The concept of splitting higher weighted particles into two parts before doing a collision process and merging them afterwards is studied in this section. The idea is to modify the merging possibilities to either conserve energy or linear momentum or something in between. Thus, consider the merging process of two particles with mass m, weights W_1, W_2 and velocities $\vec{v}_1$, $\vec{v}_2$ with the total energy

$$E = \frac{m W_1}{2} \vec{v}_1^{\,2} + \frac{m W_2}{2} \vec{v}_2^{\,2} \tag{4.5}$$

and the total momentum

$$\vec{p} = m W_1 \vec{v}_1 + m W_2 \vec{v}_2 \ . \tag{4.6}$$

The error ΔE in energy occuring by merging the two particles with two different velocities to one particle with one velocity then depends on the error Δp that is allowed in linear momentum as

$$\Delta E = E - \frac{(p - \Delta p)^2}{2m\,(W_1 + W_2)} \ . \tag{4.7}$$

For $\Delta p = 0$, the equation above is equivalent to Boyd's method (3.14). Merging the two pseudo-particles means to set their velocities such that their total energy is $E - \Delta E$ and their total linear momentum is $(1 - \Delta p/p) \cdot \vec{p}$, respectively. The functional dependence $\Delta E(\Delta p)$ can be illustrated

as in figure 4.1. The absolute value of the total linear momentum p defines the radius of the green circle. The total energy E (actually $\sqrt{2m(W_1+W_2)E}$) then defines the radius belonging to the red circle. The difference between both circles then corresponds to the energy loss ΔE in Boyd's method.

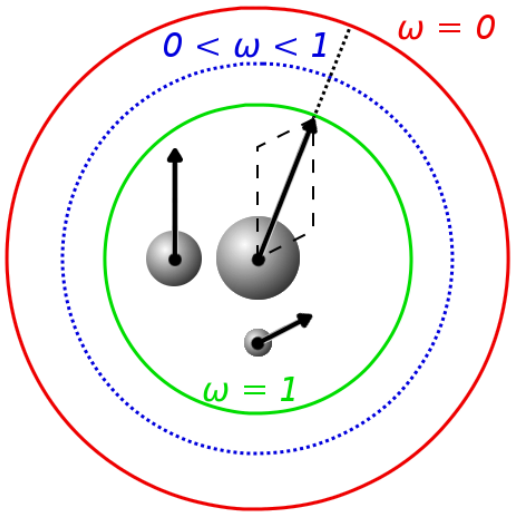

Figure 4.1.: The two small grey pseudo-particles shall be merged into the big grey pseudo-particle. If linear momentum is conserved, the new pseudo-particle's vector of linear momentum points up to the green circle ($\omega = 1$, see section (4.2.1)). If energy is conserved, it points up to the red circle instead ($\omega = 0$). For $\omega \in (0,1)$ it points somewhere in between (blue circle). For $\alpha = 1$ all circles are at the same distance. Thus, both energy and linear momentum can be conserved exactly for $\alpha = 1 \Leftrightarrow \vec{v}_1 = \vec{v}_2$ (see (4.9)).

As the solutions with minimal error in both energy and linear momentum are of interest, an error function F can be defined from the squared relative errors in linear momentum $\varepsilon := \Delta p/p$ weighted with ω and in energy weighted with $(1-\omega)$. The relative error in energy is given by (4.7) divided by E. Hence, the error function F is

$$F(\alpha, \omega, \varepsilon) = (1-\omega)\left(1-\alpha(1-\varepsilon)^2\right)^2 + \omega\varepsilon^2 \tag{4.8}$$

with

$$\alpha = \frac{p^2}{2m(W_1+W_2)E} = \left(1 + \frac{(\vec{v}_1-\vec{v}_2)^2}{\left(\sqrt{W_1/W_2}\vec{v}_1 + \sqrt{W_2/W_1}\vec{v}_2\right)^2}\right)^{-1} \in [0,1] \ . \tag{4.9}$$

As this error function is going to be minimized with respect to ε, the parameter ω allows to switch steadily between conservation of energy ($\omega = 0$) and conservation of linear momentum ($\omega = 1$). In figure 4.1 this means a continous decrease of the radius of the red circle (blue circle) to the radius of the green circle.

4.2.1. Different solutions for minimizing the error function

The minimization of the error given by F in (4.8) depending on α and ω is done by setting

$$\left.\frac{\partial F}{\partial \varepsilon}\right|_{\varepsilon_0(\alpha,\omega)} = 0 \quad \text{and} \quad F(\alpha,\omega,\varepsilon_0(\alpha,\omega)) \leq F(\alpha,\omega,\varepsilon) \ \forall \varepsilon \in \mathbb{R} \ . \tag{4.10}$$

As F is a non-negative polynomial of degree four in ε, for a given pair (α,ω) it has at least one and at most two local minima. If there is more than one local minimum only the global minimum out of the two of them has to be selected. If F is equal for both minima such that both local minima are global minima, it is of interest for which local minimum the overall error is minimal. The ε fulfilling this is from now on called $\varepsilon_{0,\omega}(\alpha)$. The minimized overall error is given by the sum of squared variation coefficients

$$\left(\frac{\Delta E}{E}\right)^2 + \left(\frac{\Delta p}{p}\right)^2 \equiv 2F\left(\alpha, \omega = \frac{1}{2}, \varepsilon_{0,\omega}(\alpha)\right) =: 2F_{1/2}\left(\alpha,\omega\right) \ . \tag{4.11}$$

Conservation of energy

For $\omega = 0$, the condition for minimization (4.10) is equivalent to conservation of energy such, that the minimal relative error in linear momentum becomes

$$\varepsilon_{0,0}(\alpha) = 1 - \sqrt{\alpha^{-1}} \leq 0 \ . \tag{4.12}$$

General solutions

For all $\omega > 40/91$ it is shown in A.1, that F is minimal at

$$\varepsilon_{0,\omega>40/91} = 1 - \left(\sqrt[3]{\frac{\overline{q}}{2} + \sqrt{\left(\frac{\overline{q}}{2}\right)^2 + \frac{1}{27\alpha^3}\left(\alpha\overline{q}-1\right)^3}} + \sqrt[3]{\frac{\overline{q}}{2} - \sqrt{\left(\frac{\overline{q}}{2}\right)^2 + \frac{1}{27\alpha^3}\left(\alpha\overline{q}-1\right)^3}} \right), \tag{4.13}$$

where

$$\overline{q} = \frac{\omega}{2\alpha^2(1-\omega)} \ , \tag{4.14}$$

substituting (A.3) into (A.2). The solution can be retained if $27\overline{q}^2 + 4\left(\overline{q} - \alpha^{-1}\right)^3 > 0$ such that the roots can be chosen real. Otherwise, the general solution is given by

$$\varepsilon_0 = 1 \mp \sqrt{\frac{4}{3}(\alpha^{-1} - \overline{q})} \cos\left(\frac{1}{3}\arccos\left(\sqrt{\frac{27\overline{q}^2}{4\left(\alpha^{-1}-\overline{q}\right)^3}}\right) + \beta\right), \tag{4.15}$$

with $\beta \in \{-\pi/3, 0\}$ so constituted that $F\left(\alpha,\omega,\varepsilon_0(\beta)\right)$ is minimal. The sign is negative if $\beta = 0$.

Conservation of linear momentum

For $\omega \to 1$ it follows $\overline{q} \to \infty$ such that (4.13) provides conservation of linear momentum $\varepsilon_{0,1} = 0$ as expected such that the relative error in energy becomes

$$\frac{\Delta E_{0,1}}{E} = \sqrt{(F(\alpha,1,0))} = 1 - \alpha \geq 0 \ . \tag{4.16}$$

Substituting α by (4.9) and E by (4.5) yields

$$\Delta E = \frac{W_1 W_2}{W_1 + W_2}\frac{m}{2}\left(\vec{v}_1 - \vec{v}_2\right)^2, \tag{4.17}$$

which is the limit of Boyd's method (3.14) with $m_1 = m$, $\widetilde{W}_2 = W_2$ and $\widetilde{W}_1 = W_1 + W_2$.

Minimal sum of the squared variation coefficients

Now, take a look at the overall error given by the sum of the squared variation coefficients $2F_{1/2}(\alpha,\omega)$. It is obvious, that this sum is minimal if $F(\alpha,1/2,\varepsilon)$ is minimal, which is given for (4.13) setting $\omega = 1/2$ in (4.14):

$$\varepsilon_{0,1/2}(\alpha) = 1 - \frac{1}{\sqrt[3]{4\alpha^2}} \left(\sqrt[3]{1 + \sqrt{1 + \frac{16\alpha}{27}\left(\frac{1}{2\alpha} - 1\right)^3}} + \sqrt[3]{1 - \sqrt{1 + \frac{16\alpha}{27}\left(\frac{1}{2\alpha} - 1\right)^3}} \right) . \tag{4.18}$$

This is the least relative error occuring in either energy or momentum. It is shown in figure 4.2, that it indeed is a minimum for any given α compared with conservation of energy ($\omega = 0$) or linear momentum ($\omega = 1$). For conservation of energy the overall error diverges for $\alpha \to 0$. This is obvious, as $\alpha \to 0 \;\Leftrightarrow\; \vec{p} \to 0$ and coincides with (4.12).

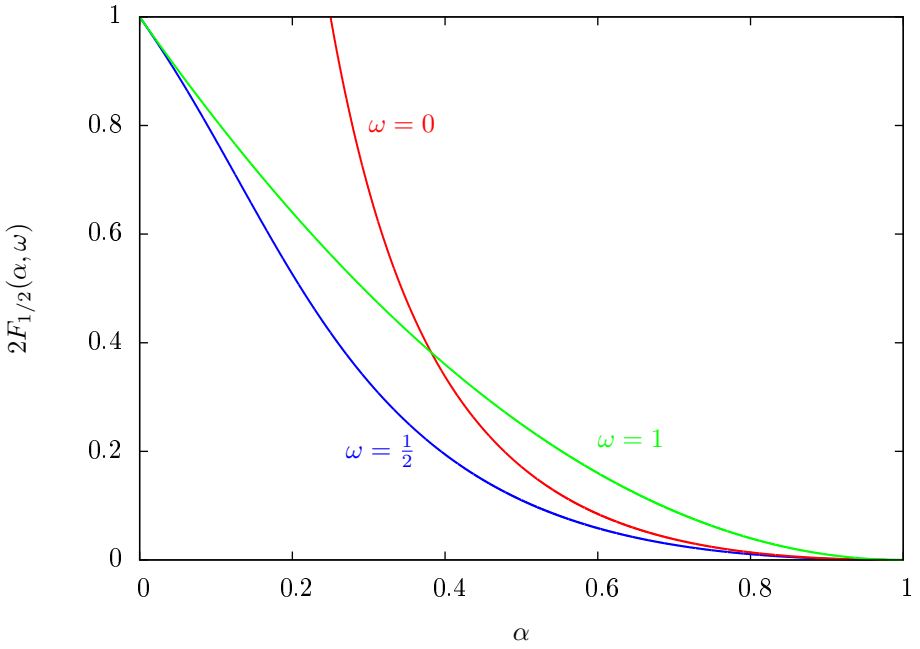

Figure 4.2.: The minimized sum of the squared variation coefficients $2F_{1/2}$ as a function of α for $\omega = 0$ (conservation of energy), $\omega = 1/2$ (minimal $F_{1/2}$) and $\omega = 1$ (conservation of linear momentum).

4.2.2. Recap of the collision process with minimal error

Using the minimized relative error $\varepsilon_{0,\omega}(\alpha)$ the collision process can be summarized. The number of selected pairs is still given by (3.7) or (3.10) to (3.12), the reaction probability by (3.8) or (3.13) and the angular distributions by (3.5) and (3.6). The post-collision velocity of the higher weighted particle $\vec{v}'_>$ is then given by the post-collision velocity of its fraction part and of its initial velocity. As the linear momentum of the merged particle is set to

$$\vec{p}'_> = (1 - \varepsilon_{0,\omega}(\alpha)) \cdot m_> \left((W_> - W_<)\,\vec{v}_> + W_< \left(\vec{v}_> \pm \frac{m_<}{m_< + m_>} \cdot \Delta\vec{v}_r \right) \right) \tag{4.19}$$

$$= (1 - \varepsilon_{0,\omega}(\alpha)) \cdot m_> \left(W_>\vec{v}_> \pm W_< \frac{m_<}{m_< + m_>} \Delta\vec{v}_r \right) \tag{4.20}$$

the post-collision velocities are

$$\vec{v}_>' = (1 - \varepsilon_{0,\omega}(\alpha)) \left(\vec{v}_> \pm \frac{W_<}{W_>} \frac{m_<}{m_< + m_>} \Delta\vec{v}_r \right) \tag{4.21}$$

$$\vec{v}_<' = \vec{v}_< \mp \frac{m_<}{m_< + m_>} \Delta\vec{v}_r \ , \tag{4.22}$$

where $_<$ defines the properties of the less weighted and $_>$ of the higher weighted pseudo-particle. The choice of the sign depends on the definition of $\vec{v}_r = \pm(\vec{v}_> - \vec{v}_<)$.

4.2.3. Correction of errors in energy and momentum

For numerical simulations it might be necessary that the errors in both energy and momentum are diagnosed and corrected in later collisions, because otherwise dissipation is created. Following Boyd's idea of adding the error in energy to the relative velocity at later collisions, the error of linear momentum can be added to the center-of-mass velocity. Therefore, consider a collision between two equally weighted pseudo-particles with weight W and mass m with post-collision velocities

$$\vec{v}_1' = \vec{v}_1 + \frac{\Delta\vec{p}}{2Wm} + \frac{\kappa}{2} \left(\hat{A} - \hat{1} \right) \cdot \vec{v}_r \tag{4.23}$$

$$\vec{v}_2' = \vec{v}_2 + \frac{\Delta\vec{p}}{2Wm} - \frac{\kappa}{2} \left(\hat{A} - \hat{1} \right) \cdot \vec{v}_r \ . \tag{4.24}$$

With this approach an error in linear momentum $\Delta\vec{p}$ that occurred in former collisions can be corrected. The parameter κ has to be chosen such that energy is conserved with respect to an error ΔE. By solving

$$\vec{v}_1'^2 + \vec{v}_2'^2 = \vec{v}_1^2 + \vec{v}_2^2 + \frac{2\Delta E}{Wm} \tag{4.25}$$

for κ, using $\vec{v}_r \cdot \hat{A}\vec{v}_r = v_r^2 \cos\theta$ and $\hat{A}\vec{v}_r \cdot \hat{A}\vec{v}_r = v_r^2$ yields

$$\kappa = \frac{1}{2} \pm \sqrt{\frac{1}{4} + \left(2\Delta E - (\vec{v}_1 + \vec{v}_2)\,\Delta\vec{p} - \frac{\Delta\vec{p}^2}{2Wm} \right) \cdot \left(\frac{1}{Wmv_r^2\,(1 - \cos\theta)} \right)} \ , \tag{4.26}$$

where θ is the scattering angle. The case $\Delta E = \Delta\vec{p} = 0$ delivers $\kappa = 1$, so (4.23) and (4.24) are identical to (2.11) and (2.12). Hence, the negative sign is not reasonable as for $\Delta E = \Delta\vec{p} = 0$ there would be no collision ($\vec{v}_1' = \vec{v}_1$ and $\vec{v}_2' = \vec{v}_2$). It is obvious that this correction should be done at collisions between highly weighted particles (W large) since then the relative correction is small as the terms of correction are proportional to W^{-1}. Moreover, it is important to note that the radicand might become less than zero. To avoid this ΔE can be increased such that the root becomes zero. The difference $\Delta E'$ then becomes the new error in energy for this collision.

5. Numerical results for a 1D simulation

In the following some numerical tests are performed for the DSMC procedure. The output is generated by a C-program that uses different collision methods for non-linear DSMC simulating a gas in a pipe. The program is one-dimensional in position-space such that the pushing of the pseudo-particles in axial direction (z-direction) is performed, but the pushing in perpendicular direction is ignored. In velocity-space the gas is simulated three-dimensional as the description of the binary collisions requires this. With the numerical tests the behaviour of conserved quantities and distribution functions for different collision methods will be examined and it will be shown to what extent relaxation processes in gases with different weights coincide with a reference test with equal weights.

5.1. Evolution of a Maxwell-distributed gas

As a first numerical test a Maxwell-distributed gas is considered with density $n = 10^{19}\,\mathrm{cm}^{-3}$ and temperature $T = 300\,\mathrm{K}$ containing two types of Argon pseudo-particles. The first type is weighted with $W_1 = 2.4$ and the second with $W_2 = 100\,W_1$. Each type has 200000 pseudo-particles. The gas is spread homogeneously in the pipe of radius $r = 5\,\lambda_{\mathrm{mfp}}$ and length $z_{\max} = 25000\,\lambda_{\mathrm{mfp}}$ divided into 5000 cells. The boundary condition in z-direction is set periodically. As the initial gas is already in thermodynamic equilibrium nothing should happen to the gas' distribution functions for 100 timesteps of $0.5\,\tau$. In the following, the four collision methods (direct collisions, $\omega = 0$, $\omega = 1/2$ and $\omega = 1$) are compared varying the method of selecting pairs of pseudo-particles once with and once without correction of conservation.

5.1.1. Unsorted selection of pairs without correction

At first, the pairs of pseudo-particles are combined without paying attention to the weight of the pseudo-particles, but with modified reaction probability. Moreover, no correction of any error which arises from the merging process is performed. Doing so, one gets distribution functions shown in figure 5.1.
One can see that for conservation of linear momentum (a)), which is Boyd's method without conservation of energy, the qualitative behaviour for both low and high weighted pseudo-particles' distribution functions is still conserved after 100 timesteps, but quantitative differences appear. This is evident as the merging process is accompanied by dissipation, which is confirmed by the time-evolution of the relative error in energy shown as green line in figure 5.2.
For conservation of energy (b)) the qualitative behaviour of the distribution function after simulation is only similar to the start distribution for the low weighted particles (red points). For the high weighted pseudo-particles the distribution function shows a strong drop for low absolute values in velocity. This becomes clear remembering that an error is created in the merging process for each collision between differently weighted pseudo-particles. As the merging process for $\omega = 0$ always leads to an increase of absolute value of linear momentum, the mean absolute value of velocity for the high weighted particles increases with each time step. The case $\omega = 1/2$ (c)) can be understood as a superposition of $\omega = 0$ and $\omega = 1$. For this, it is important to note that the developments of the relative error in linear momentum might be different, because the absolute value of $\langle p_z \rangle(0)$ is close to zero. Therefore, the relative error in linear momentum is susceptible to slight deviations in linear momentum. For many collisions the error manifests itself and propagates on average to an increasing relative error into a preferred direction.
Finally, consider the direct collisions. One can see, that the distribution function of the high weighted pseudo-particles is still close to Maxwellian, while the low weighted pseudo-particles

are uniformly distributed. As the weights between the particles are very different, a collision between one low and one high weighted particle induces on average an energy transfer from the high to the low weighted particle (see (4.2) and (4.3) for $W_2 \gg W_1$). This leads to a severe heating of the low and to a slight cooling of the high weighted pseudo-particles.

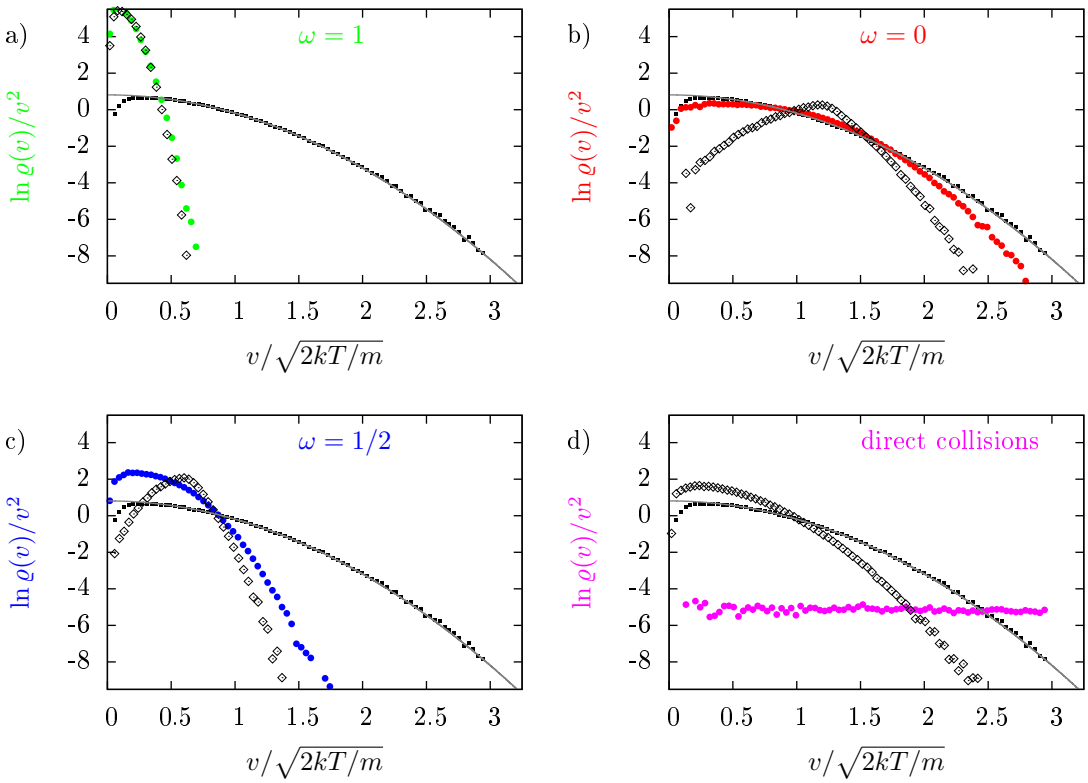

Figure 5.1.: The velocity distribution function at time $t = 50\,\tau$ for the low weighted particles W_1 (coloured points), for the high weighted particles $W_2 = 100\,W_1$ (black bounded diamonds), the overall velocity distribution function at time $t = 0$ (black squares) and its theoretical behaviour (grey line) for the four collision methods.

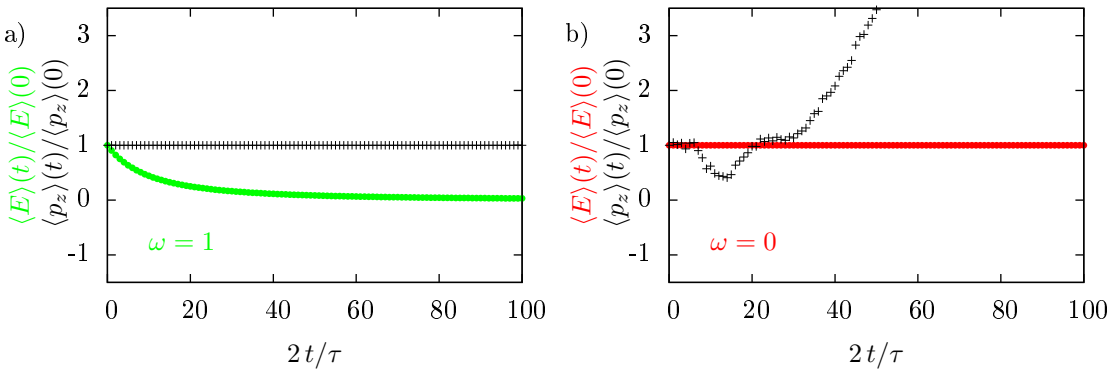

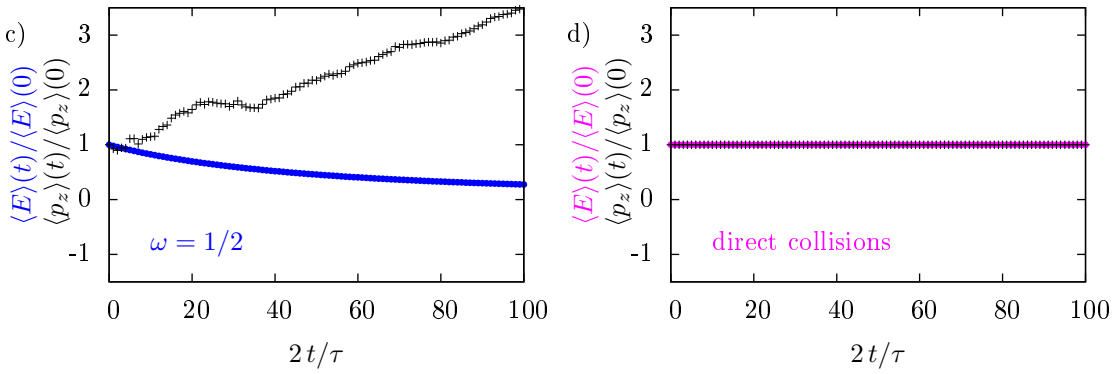

Figure 5.2.: The time evolution of the relative error in energy (coloured line) and of the z-component of linear momentum (black crosses) for the four collision methods.

5.1.2. Unsorted selection of pairs with correction

Now, the collision method is changed by correcting the error according to (4.23) and (4.24). As this does not change anything for the method of direct collisions and because the case $\omega = 1/2$ is in essence some kind of superposition of the cases $\omega = 0$ and $\omega = 1$, both cases are left out here. It can be seen in figure 5.3 a) that linear momentum is again conserved exactly and that the relative energy does not approach to zero but to a constant value. Its difference from one can be explained by the fact that it is not granted that each high weighted pseudo-particle that loses energy will collide in the same time step again with another high weighted pseudo-particle. Hence, at least a small part of energy loss will be carried from one time step to the next with the result that for many time steps the relative energy converges to a fixed value. It can be argued very similar for case b) with the difference, that the error in linear momentum occurs in all directions with the same probability. Hence, linear momentum is conserved on average over a large amount of collisions.

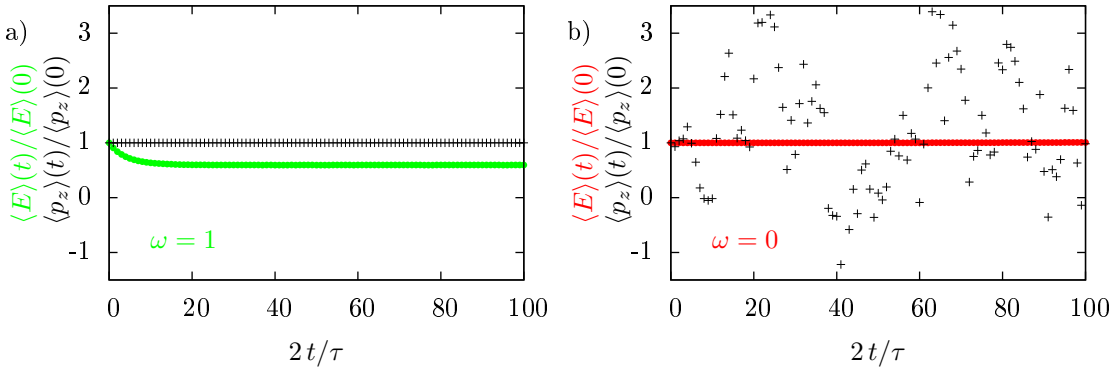

Figure 5.3.: The time evolution of the relative error in energy (coloured line) and of the z-component of linear momentum (black crosses) for the two collision methods.

Now, considering the distribution functions, there are the same errors as in the non-conserving method discussed before but now at steady state: after a sufficiently long time there is no loss in temperature anymore for a). This is recognizable by detecting the different stretching factors of the parabolas in a) after the same runtime, which agrees with figure 5.3 a).

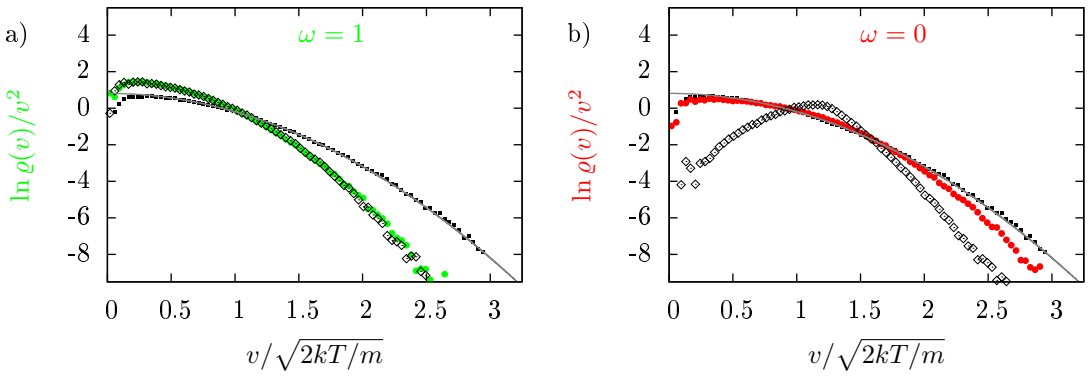

Figure 5.4.: The velocity distribution function at time $t = 50\,\tau$ for the low weighted particles W_1 (coloured points), for the high weighted particles $W_2 = 100\,W_1$ (black bounded diamonds), the overall velocity distribution function at time $t = 0$ (black squares) and its theoretical behaviour (grey line) for the two collision methods.

5.1.3. Sorted selection of pairs without correction

The next modification of the collision method is done without correction of the errors, but with sorted pairs. This means that at first the collisions between two low weighted pseudo-particles are performed followed by the collisions with different weights and finally by the collisions with high weights.

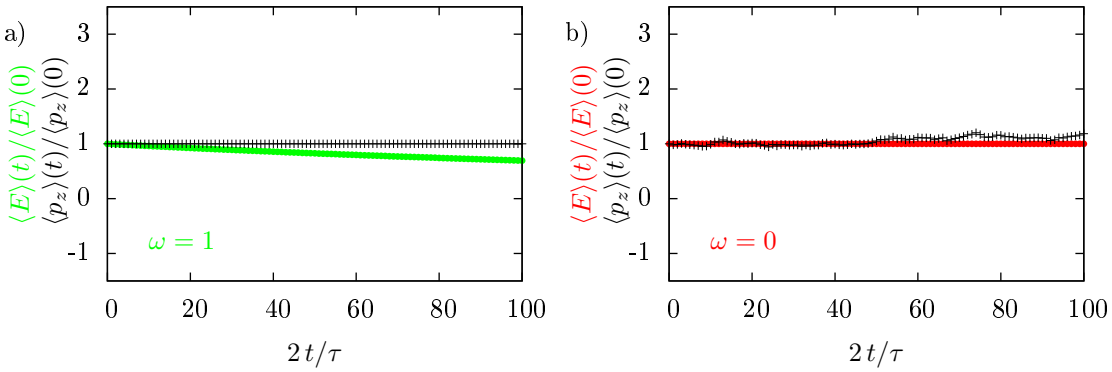

Figure 5.5.: The time evolution of the relative error in energy (coloured line) and of the z-component of linear momentum (black crosses) for the two collision methods.

Comparing the relative errors in figure 5.5 to figure 5.2, a severe reduction of the error after the same number of time steps can be detected. This is obvious, because the number of collisions between pseudo-particles with different weight, which cause the error, are proportional to

$$\langle N_c\rangle^{1\leftrightarrow 2} \propto \frac{1}{2}\frac{(N_1+N_2)^2}{2} \tag{5.1}$$

for the unsorted, and

$$\langle N_c\rangle^{1\leftrightarrow 2} \propto N_1 \cdot N_2 \tag{5.2}$$

for the sorted method. As in the given example the ratio of the number of real particles $N_2/N_1 = 100$, there are more than 25 times more collisions between differently weighted particles using the unsorted method than using the method of sorted pairs. This reduction of the error can also

be seen at the distribution functions in figure 5.6. Now there is only a slight error in temperature for a) and in contrast to the conserving method with unsorted pairs almost no error for b).

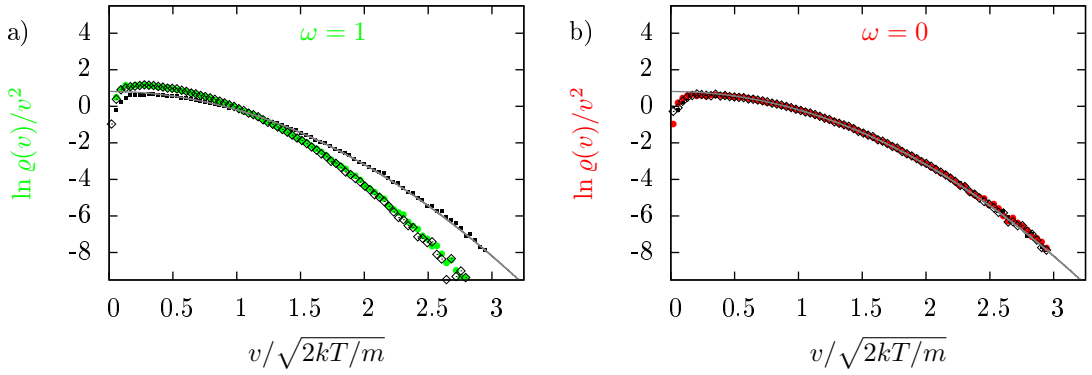

Figure 5.6.: The velocity distribution function at time $t = 50\,\tau$ for the low weighted particles W_1 (coloured points), for the high weighted particles $W_2 = 100\,W_1$ (black bounded diamonds), the overall velocity distribution function at time $t = 0$ (black squares) and its theoretical behaviour (grey line) for the two collision methods.

5.1.4. Sorted selection of pairs with correction

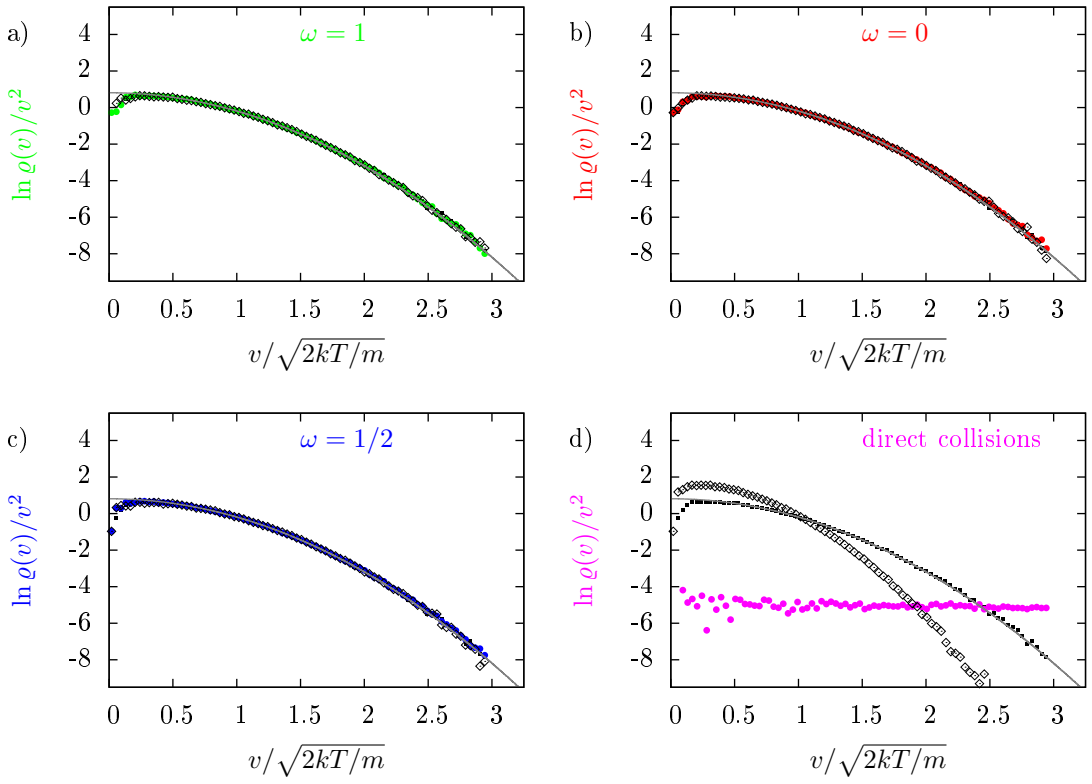

Figure 5.7.: The velocity distribution function at time $t = 50\,\tau$ for the low weighted particles W_1 (coloured points), for the high weighted particles $W_2 = 100\,W_1$ (black bounded diamonds), the overall velocity distribution function at time $t = 0$ (black squares) and its theoretical behaviour (grey line) for the four collision methods.

As a last step both collision methods are combined. Now the pseudo-particles are sorted for dividing them into pairs and the errors arising for collisions between differently weighted particles are corrected afterwards during the same time step, when the collisions between the high weighted particles are performed. For this, the case $\omega = 1/2$ is retrieved and also the influence of sorted pairs on direct collisions is going to be tested.

As shown in figure 5.7 the distribution functions are retained for all collision methods except direct collisions. Here, there is no influence of sorted pairs, at least not if the collisions between the low weighted pseudo-particles are performed before the collisions of the differently weighted pseudo-particles. The conservation of the distribution functions also agrees with the conservation of both energy and linear momentum, shown in figure 5.8.

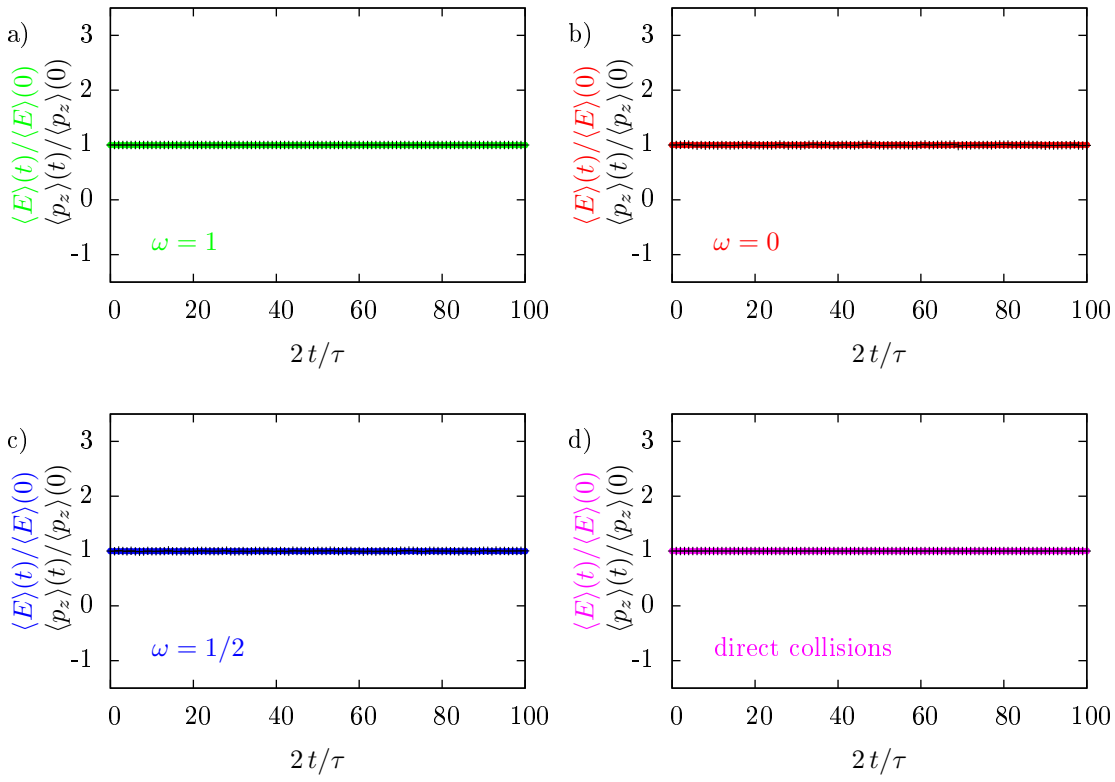

Figure 5.8.: The time evolution of the relative error in energy (coloured line) and of the z-component of linear momentum (black crosses) for the four collision methods.

5.2. Evolution of a Maxwell-distributed gas with beam

As a next step the initial velocity in z-direction is increased about $v_0 = \sqrt{32\,k_B T/(\pi m)}$, such that there is a beam of particles in z-directions. Therefore, it is of interest if the anisotropic distribution function

$$\varrho_z(v_z) = \sqrt{\frac{m}{2\pi k_B T}} \cdot \exp\left(-\frac{m\,(v_z - v_0)^2}{2k_B T}\right) \tag{5.3}$$

is retained for the four collision methods with sorted pairs and correction in both energy and linear momentum. Since there are periodic boundaries it is expected that the beam in thermodynamic equilibrium is retained very well.
It can be seen in figure 5.9 that the anisotropic distribution functions are retained for all methods except for direct collisions, for which the different weights are treated as different masses. For this method, the deviation is very similar to that of the test without beam. The uniform distribution of the low weighted particles can not be seen, because only the overall distribution function is plotted, which is dominated by the high weighted pseudo-particles.

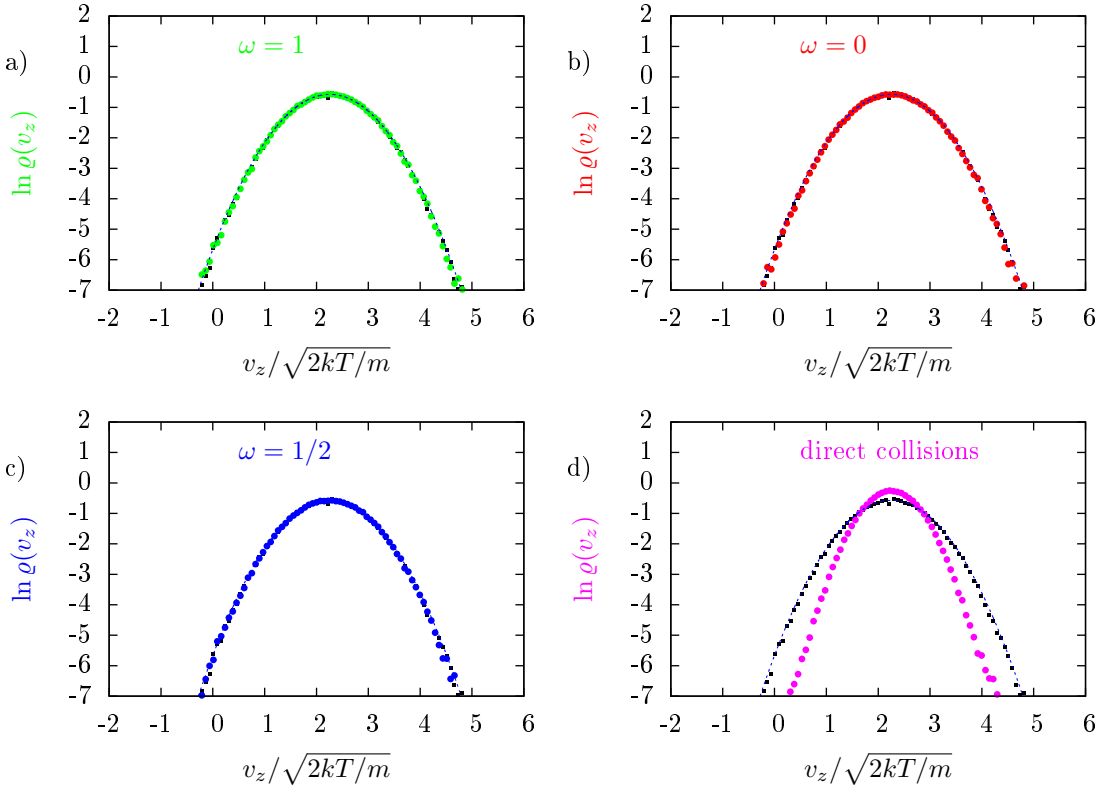

Figure 5.9.: The z-fraction part of the overall velocity distribution function at time $t = 50\,\tau$ (coloured points), at time $t = 0$ (black squares) and its theoretical behaviour (grey line) for the four collision methods.

5.3. Relaxation of a gas with elliptic velocity distribution function

As a next test a relaxation process of Maxwell-distributed gas with different temperatures in axial and perpendicular directions is examined. The initial velocity distribution function is

$$\varrho(v_\perp, v_z) = \left(\frac{m}{2\pi k_B}\right)^{3/2} \cdot T_\perp^{-1} \cdot T_z^{-1/2} \cdot \exp\left(-\frac{m v_\perp^2}{2k_B T_\perp}\right) \exp\left(-\frac{m v_z^2}{2k_B T_z}\right) \quad . \tag{5.4}$$

Since this is not the equilibrium distribution function, it will take some time for the system to relax. The relaxation time should be independent of the particles weights if the physical conditions are the same. Hence, the total number of both real and pseudo-particles are not modified, but only both weights W_1 and W_2 instead. The exponential fits of the results in figure 5.10 show ratios $\widetilde{\tau}_1/\widetilde{\tau}_{1000} \simeq 20$ of the relaxation times $\widetilde{\tau} = t/\ln\left(\Delta T(0)/\Delta T(t)\right)$ of a system with equally weighted pseudo-particles ($W_2/W_1 = 1$) and one with weight ratio $W_2/W_1 = 1000$.

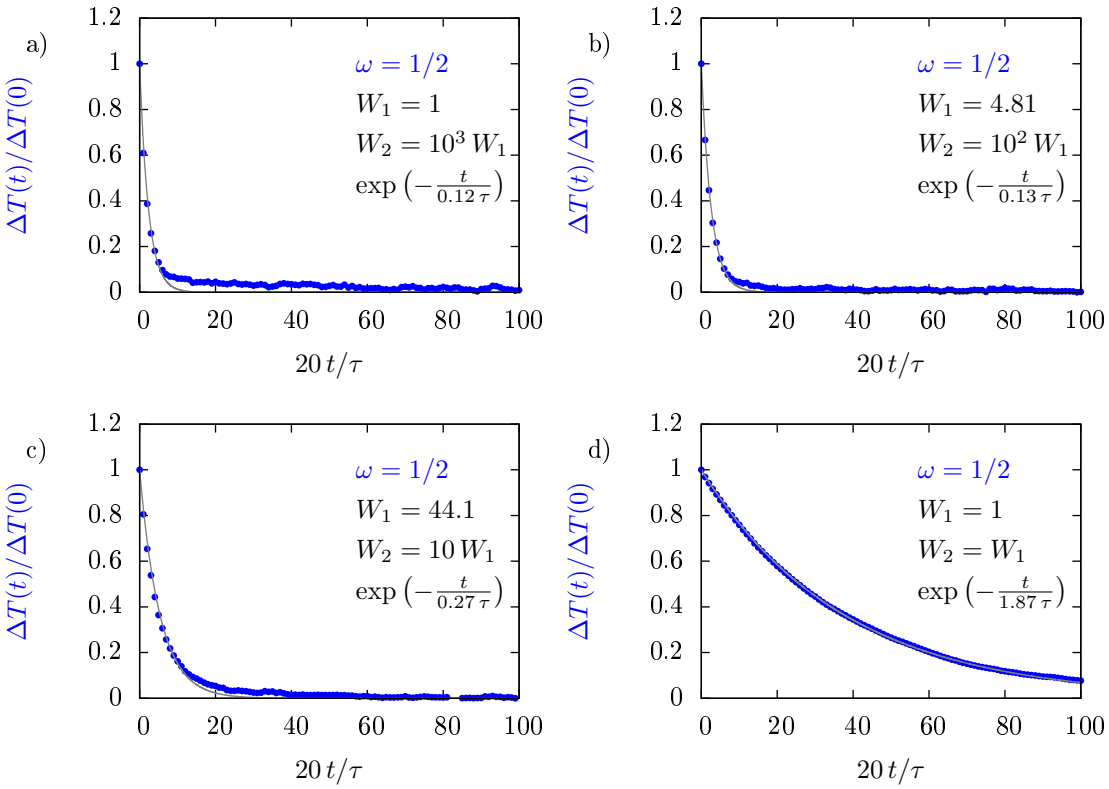

Figure 5.10.: The time evolution of the relative temperature difference of axial and perpendicular temperatures (blue points) and its exponential fit (grey line).

Although here only the results for $\omega = 1/2$ are shown the other methods produce for the same pseudo-particle weights the same relaxation times, even for direct collisions. This indicates that collisional effects are too strong and the calculation of the number of pairs has to be adjusted. Probably, the weigths of individual collisions for the different collision categories have to be modified to guarantee the correct physical scaling. This is rather complicated, because a mix of collisions between large weighted particles, between large and small weighted particles and between small weighted particles appears simultaneously in the algorithm. The individual scaling factors for these different collisions have to be determined analytically such that the same

collisional effects (and by this the same relaxation times) are produced like in the case of individual real particles. This work is beyond the scope of this thesis, but will be the topic of future research to turn the approach developed here into a practical algorithm applicable in complex simulations. Such numerical artefacts appear also in a test case with self-diffusion of the gas with different weights shown in A.2

6. Conclusions and outlook

The extension of DSMC for systems with trace species requires non-linear weigthing schemes and the accomplishment of collisions between differently weighted pseudo-particles. Advantages and disadvantages of different approaches have been compared. One of the methods enforces both energy and linear momentum conservation by treating the different weights as different masses performing direct collisions, but does not guarantee a Maxwellian distribution function in equlibrium. The others use splitting of pseudo-particles with large weights into smaller weights for collisions with lower weighted particles. A merging process performed afterwards causes an error in either energy or linear momentum or both. This error can be minimized further for individual collisions. In the statistical limit of a large number of collisions this error per time step depends on the number of collisions between differently weighted pseudo-particles.

To obtain the right number of collisions there are different ways to calculate the number of pairs considered for collisions and their reaction probabilities. One possibility is to modify the reaction probability, but not the number of pairs. However, this does not reduce the number of pairs compared with equally weighted pseudo-particles, and the number of collisions between two differently weighted pseudo-particles is very large. This causes a large error in energy or linear momentum. Alternatively, the number of pairs is modified by sorting them according to their weights without changing the reaction probability. However, this method is only applicable for a large number of pseudo-particles with equal weights. Otherwise it is at the expense of statistical accuracy.

A general observation is that a Maxwellian distribution function can not be obtained after a large number of timesteps if the error caused by the merging process is not corrected. This correction can be done in later collisions between pseudo-particles with large weights. If the ratio of the different weights is of the order of $W_2/W_1 \ll 10^2$ problems occur for methods that do not conserve linear momentum: a further correction can not be implemented for all cases, as there might arise some negative radicants. These can only be introduced as zeros resulting in energy errors.

The collision methods using splitting and merging for sorted pairs with correction conserve energy and linear momentum very well and guarantee a Maxwellian distribution even for test cases where particle beams are used. However, even if the qualitative development of the systems considered look good, a full quantitative correct time evolution of physical systems is not guaranteed. The most promising approach is Boyd's method of conserving linear momentum exactly and adding the error in energy to the relative velocity. In addition, there are no problems in correcting the error for low weight ratios in contrast to all other approaches. Therefore, it is recommended to set the focus on this method for further applications.

In realistic applications, additional complications arise due to other processes, such as ionization and charge-exchange. If a low weighted electron collides with a high weighted neutral pseudo-particle it can perform an electron impact ionization. This creates a broader distribution of weights by reducing the weight of neutrals subsequently in each ionization. The same holds for charge-exchange collisions coupling the different weight distributions of ions and neutrals. Therefore, it will be necessary to develop non-linear DSMC for broad distributions of pseudo-particle weights. A possible ansatz can be to introduce variable boundary values for categorization of low and high weight particles. It might be useful to mix both modifications of number of pairs and reaction probability. The groups of pseudo-particles for the different categories of low and high weight would then be defined by different thresholds.

A. Appendix

A.1. Minimization of the error function

The function that yields the error occuring in energy and momentum by merging particles is given by

$$F(\alpha, \omega, \varepsilon) = (1-\omega)\left(1-\alpha\left(1-\varepsilon\right)^2\right)^2 + \omega\varepsilon^2 \ . \tag{A.1}$$

Its minimum, which is dependent on the particles parameter α and the weighting ω of the error in momentum in relation to the whole error, can be found by setting the derivative with respect to ε to zero, which is equivalent to

$$(1-\varepsilon)^3 - \left(\frac{1}{\alpha} - \frac{\omega}{2\alpha^2(1-\omega)}\right)(1-\varepsilon) - \frac{\omega}{2\alpha^2(1-\omega)} = 0 \ .$$

This equation is of the form $r^3 + k \cdot r + q = 0$, which has exactly one real solution[8]

$$r = \sqrt[3]{-\frac{q}{2} + \sqrt{D}} + \sqrt[3]{-\frac{q}{2} - \sqrt{D}} \tag{A.2}$$

if the discriminant

$$D = \left(\frac{q}{2}\right)^2 + \left(\frac{k}{3}\right)^3 \geq 0 \ . \tag{A.3}$$

This means that the roots in the equation are real roots. This can be proven by substituting r and D into the initial equation and by showing that multiplying the individual summands in (A.2) with the two different complex third roots of unity yields two more truly complex solutions. To get dependencies for α and ω such that D is greater than zero, consider

$$D = \left(\frac{q}{2}\right)^2 \left(1 + \frac{4k^3}{27q^2}\right) > 0 \ .$$

Hence follows $27q^2 > -4k^3$ which is equivalent using $k = -q - \alpha^{-1} =: \overline{q} - \alpha^{-1}$ to

$$27\overline{q}^2 + 4\left(\overline{q} - \alpha^{-1}\right)^3 > 0 \ . \tag{A.4}$$

As the parameters ω and α have to be chosen from (0,1), $\overline{q} = \omega/(2\alpha^2(1-\omega)) \geq 0$, so (A.4) can be complied with by

$$27\overline{q}^2 > \frac{4}{\alpha^3} \ . \tag{A.5}$$

Substituting $\overline{q}$ yields

$$\frac{\omega}{1-\omega} > \frac{4}{\sqrt{27}}\sqrt{\alpha} \tag{A.6}$$

which due to $\omega \in (0,1)$ is equivalent to

$$\omega > \frac{1}{1 + \frac{\sqrt{27}}{4\sqrt{\alpha}}} \ , \tag{A.7}$$

which is fullfilled for any α if

$$\omega > \frac{40}{91} \qquad \text{as} \qquad \frac{40}{91} = \frac{4}{4 + 3\frac{17}{10}} > \frac{1}{1 + \frac{\sqrt{27}}{4}} \geq \frac{1}{1 + \frac{\sqrt{27}}{4\sqrt{\alpha}}} \ . \tag{A.8}$$

A.1.1. General solution for numerical calculations

If the discriminant can be calculated numerically for given values of α and ω, the solution can be generalized using $q \leq 0$ to [8]

$$r = \pm\sqrt{-\frac{4}{3}k}\cos\left(\frac{1}{3}\arccos\left(\sqrt{\frac{q^2}{q^2-4D}}\right)+\beta\right), \tag{A.9}$$

where β is $\pm\pi/3$ or 0 and the sign is positive, if $\beta = 0$. As in this case there are two local minima and one local maximum it has to be guaranteed that the second derivative of F with respect to ε is greater than zero, which is equivalent to

$$r^2 > \frac{2\alpha(1-\omega)-\omega}{6\alpha^2(1-\omega)} = -\frac{k}{3} \ .$$

Deliberations about possible values of the arcusfunction lead us to

$$r^2 \in -\frac{4}{3}k \cdot \begin{cases} \left[0, \frac{1}{4}\right] & \beta = \frac{\pi}{3} \\ \left[\frac{1}{4}, \frac{3}{4}\right] & \beta = -\frac{\pi}{3} \\ \left[\frac{3}{4},1\right] & \beta = 0 \end{cases} \ .$$

Hence $\beta = \frac{\pi}{3}$ is the local maximum. Considering the special cases $\omega = 0$ or $\omega \geq 40/91$ it is clear, that $1 - \varepsilon_0 = r < 0$ for the first case and $r > 0$ for the second case. As the cosine is for any relevant case non-negative, the parameter β determining the global minimum of F changes at least one time from $-\pi/3$ to 0 when ω is increased from 0 to 1. Thus the remaining solutions ($\beta = -\pi/3$ and $\beta = 0$) have to be substracted from one and the result has to be substituted as ε_0 into (A.1) to compare them to get the global minimum for a given pair of α and ω.

A.2. Diffusion

According to the third law of thermodynamics a temperature of absolute zero can never be achieved [4]. This is why particles in a fluid are always in motion. This motion is named after its discoverer as Brownian motion. It causes a mingling of the particles, which is called *diffusion*, and regarding particle interactions it leads to assimilation of the particle properties up to a *relaxation to thermodynamic equilibrium*. The process of diffusion is described by the diffusion equation, which is obtained from Fick's first law and the continuity equation [4] [6]:

$$\frac{\partial n}{\partial t} = \nabla \cdot \hat{D}\nabla n \ . \tag{A.10}$$

The factor $\hat{D}$ is called *diffusivity*, which is in general a symmetric second-order tensor and a function of time and space. If only the diffusion along one of the main axes is of interest and if the diffusion coefficient is independent of space, the diffusion equation reduces to

$$\frac{\partial n}{\partial t} = D_z \frac{\partial^2 n}{\partial z^2}, \tag{A.11}$$

where D_z is the *diffusion coefficient* along the z-axis given by [4]

$$D_z = \frac{\Delta z^2}{2\Delta t} \ . \tag{A.12}$$

Here, Δz defines the mean step of movement in z-direction during the time interval Δt. If the initial condition is $n(t = 0) = \Theta(z)$, where Θ is the Heaviside step function, and boundary conditions $n(z \to -\infty) \to 0$ and $n(z \to \infty) \to n_0$, the solution of the diffusion equation with constant diffusion coefficient D_z is given by the error function [4]

$$n(z,t) = \frac{n_0}{2}\left(1 + \operatorname{erf}\left(\frac{z}{2\sqrt{D_z t}}\right)\right) \ . \tag{A.13}$$

Such a diffusion case is used to test the influence of different pseudo-particle weights. For reasons of statistical significance and computation time a pipe of length $1200\,\lambda_{\mathrm{mfp}}$ is divided into 62 cells of size $20\,\lambda_{\mathrm{mfp}}$ each. The temperature is 300 K and the density is $n = 10^{19}\,\mathrm{cm}^{-3}$. In the first 31 cells, a Maxwell-distributed set of 363636 pseudo-particles with weight $W_1 = 106$ is inserted. In the second 31 cells there are 36363 pseudo-particles with weight $W_2 = 10\,W_1$ at the beginning. The numbers of pseudo-particles are chosen in order to have the same number of real particles of each kind and because the number of pseudo-particles is limited due to computational effort to 400000. As a reference test the weights are set to $W_1 = W_2 = 193$ and the number of pseudo-particles to 200000 for each kind. After 1000 timesteps of $5\,\tau$, an error function similar to (A.13) can be fitted to the density distribution of each kind. By comparison of the diffusion coefficients to the reference test the quality of the simulation methods can be estimated.

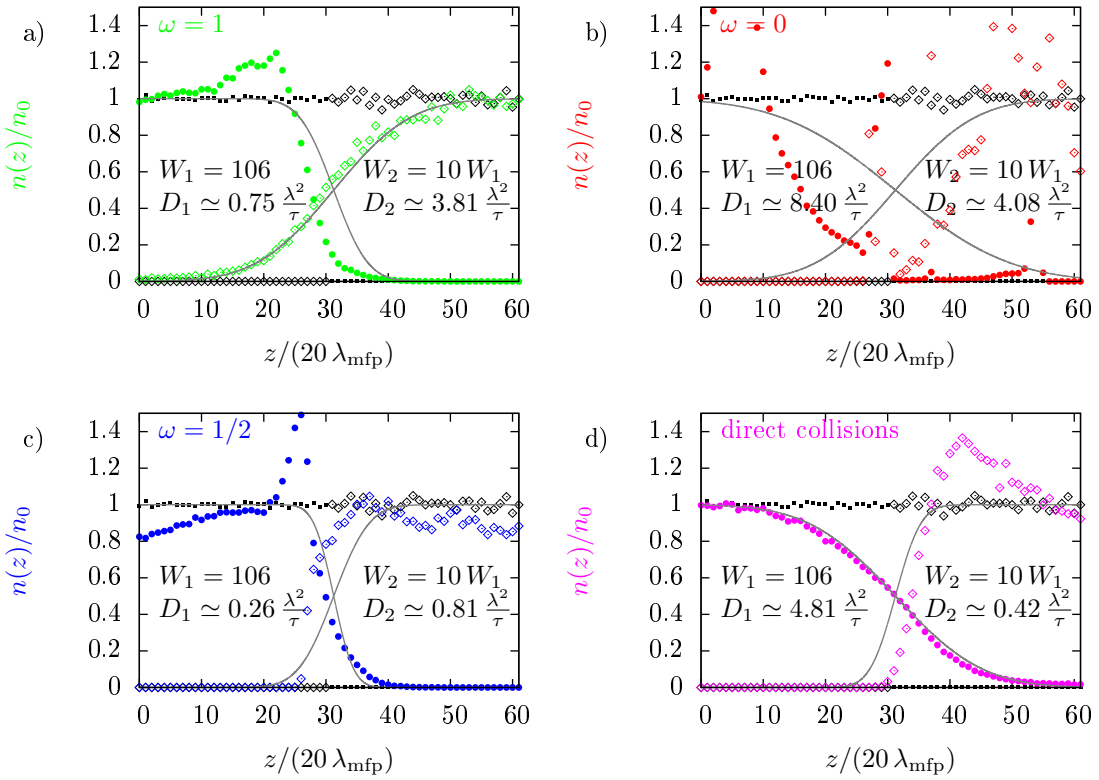

Figure A.1.: The relative particle densities of the low weighted (filled points, left) and of the high weighted pseudo-particles (bounded diamonds, right) at time $t = 0$ (black) and $t = 5000\,\tau$ (coloured) with their via D_z fitted error-function according to (A.13) (grey line).

In figure A.1 b) a large deviation of the density distribution functions to the fitted curves can be seen. Also, for $\omega = 0$ the energy increases after some time which comes from some negative radicants in (4.26). As mentioned above, these radicants can be set to zero, producing an additional error in energy $\Delta E' < 0$. Hence, for a low weight ratio ($W_2/W_1 = 10$) there is a growth of energy after some time.

However, for equally weighted pseudo-particles the system shows the expected behaviour (see figure A.2). The solution is given by (A.13) as

$$\frac{n(z,t)}{n_0} = \frac{1}{2}\left(1 + \mathrm{erf}\left(\frac{z - z_0}{2\sqrt{D_z t}}\right)\right) \tag{A.14}$$

with $z_0 = 620\,\lambda_{\mathrm{mfp}}$ and $D_z \simeq 1.2 \cdot 10^{-5}\,\mathrm{m^2 s^{-1}}$, which is of realistic order for a gas.

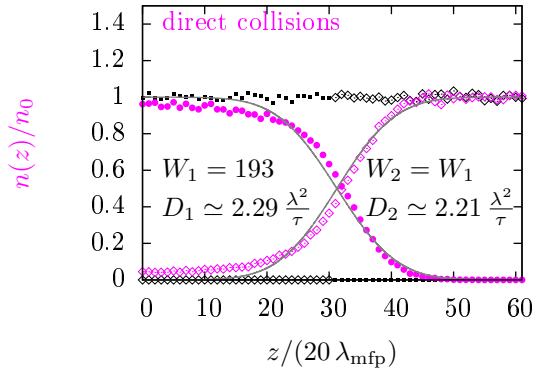

Figure A.2.: The relative particle densities of the first (filled points, left) and of the second half of the equally weighted pseudo-particles (bounded diamonds, right) at time $t = 0$ (black) and $t = 5000\,\tau$ (magenta) with their via D_z fitted error-function according to (A.13) (grey line).

It is not trivial to explain the deviations of the density distribution functions in figure A.1 from the one in figure A.2. It seems like the different species of pseudo-particles behave like species with different diffusion coefficients, which leads to density fluctuations, that are accompanied by spatial dependencies in the diffusion coefficients.

This coincides with the weight-dependent behaviour of the relaxation time in 5.3. In both cases, too many collisions compared with the real system are performed for the high weighted pseudo-particles which leads to unrealistic quantitative time evolution of physical systems.

Bibliography

[1] G. A. Bird. *Molecular Gas Dynamics and the Direct Simulation of Gas Flows*. Oxford Science Publications, 1994.

[2] Iain Boyd. Conservative Species Weighting Scheme for the Direct Simulation Monte Carlo Method. *Journal of Thermophysics and Heat Transfer*, 10(4):579–585, 1996.

[3] C.K. Oh E.S. Oran and B.Z. Cybyk. DIRECT SIMULATION MONTE CARLO: Recent Advances and Applications. *Annual Reviews of Fluid Mechanics*, 30(1):403–441, 1998.

[4] Klaus Fesser. Thermodynamik und Statistische Physik. Lecture at Ernst-Moritz-Arndt-Universität Greifswald, 2014.

[5] Konstantin Matyash. *Kinetic Modeling of Multi-Component Edge Plasmas*. PhD thesis, Ernst-Moritz-Arndt-Universität Greifswald, 2003.

[6] Hans-Erich Wagner. Physikalisches Praktikum P1. Practical training at Ernst-Moritz-Arndt-Universität Greifswald, 2011.

[7] http://jila.colorado.edu/∼avp/collision_data/neutralneutral/atomatom.txt, March 2014.

[8] Rmcharb. http://de.wikipedia.org/wiki/Cardanische_Formeln, April 2014.

Acknowledgements

At this point, I want to express my gratitude to all the people, who have supported me in writing this bachelor thesis. I would particularly like to thank Prof. Dr. Ralf Schneider for supervising my work contributing valuable expertise and experience and motivating me with his sense of purpose. Furthermore I appreciate the working climate in the research group Computational Science, which made me feel comfortable with asking questions and discussing parts of the topic. The variety of very different conversations has been very inspiring for me. I thank the members of the research group for the daily cup of coffee in good company making me feel related to the group. Besides, I want to thank my family and my female partner Sylvia for financial and emotional support. I would also like to express my special thanks to all the people, who reviewed this thesis with interest and commitment, above all Prof. Dr. Ralf Schneider, followed by Dr. Oleksandr Kalentev, Julia Duras, Karl Felix Lüskow, Lars Lewerentz and last but not least my father Dieter Klingelhöfer as the only layman with regard to DSMC. Finally, thank *you* very much for your interest in my thesis!